Published in final edited form as:
Lab Chip. 2013 May 7; 13(9): 1803–1809. doi:10.1039/c3lc41202d.

Universally applicable three-dimensional hydrodynamic microfluidic flow focusing

Yu-Jui Chiu[a], **Sung Hwan Cho**[d], **Zhe Mei**[b,c], **Victor Lien**[e], **Tsung-Feng Wu**[a], and **Yu-Hwa Lo**[a,b]

Yu-Jui Chiu: fenixroger@gmail.com

[a]Materials Science Program, University of California at San Diego, La Jolla, California 92093-0418, USA. Fax: +1-8585342486; Tel: +1-8588222777

[b]Department of Electrical and Computer Engineering, University of California at San Diego, La Jolla, California 92093-0407, USA. Fax: +1-8585342486; Tel: +1-8588222777

[c]School of Information and Electronics, Beijing Institute of Technology, Beijing 100081, China

[d]NanoCellect Biomedical Inc., 7770 Regents Road #113390, San Diego, California 92122, USA

[e]NANO3 Lab at CalIT2, University of California at San Diego, La Jolla, California 92093-0407, USA

Abstract

We have demonstrated a microfluidic device that can not only achieve three-dimensional flow focusing but also confine particles to the center stream along the channel. The device has a sample channel of smaller height and two sheath flow channels of greater height, merged into the downstream main channel where 3D focusing effects occur. We have demonstrated that both beads and cells in our device display significantly lower CVs in velocity and position distributions as well as reduced probability of coincidental events than they do in conventional 2D-confined microfluidic channels. The improved particle confinement in the microfluidic channel is highly desirable for microfluidic flow cytometers and in fluorescence-activated cell sorting (FACS). We have also reported a novel method to measure the velocity of each individual particle in the microfluidic channel. The method is compatible with the flow cytometer setup and requires no sophisticated visualization equipment. The principles and methods of device design and characterization can be applicable to many types of microfluidic systems.

Introduction

Microfluidics provides a favorable platform for biological assays because of its fluidic properties and compatible scale with biological samples such as functionalized beads, cells, and biomolecules. One prominent microfluidic biomedical assay is flow cytometer. Flow cytometers have been widely used in biomedical research and increasingly in clinical diagnosis. Flow cytometers offer a quantitative and non-invasive method to optically interrogate single cells to obtain valuable information.[1–4] In clinics, flow cytometers help diagnose and monitor diseases such as AIDS and leukemia.[5–7] The use of microfluidic devices to replace conventional flow chambers for flow cytometers offers the advantage of reduced cost, size, cross contamination, and volume of reagents and wastes.[8,9] Microfluidics also helps translate flow cytometer and other flow-based health systems (*e.g.* complete blood count systems, Coulter counters, *etc.*) to point-of-care clinics. One common and

Correspondence to: Yu-Jui Chiu, fenixroger@gmail.com.

important feature shared by many flow systems for biomedicine is flow confinement. By keeping the biological samples near the center of the channel, one can reduce the chance of channel clogging, sample fouling or absorption to the channel wall, coincidental errors, and non-uniformity in the speed of travel. Coincidental errors occur when more than one cell passes the interrogation area at the same time. With coincidental events and cell speed non-uniformity, the accuracy and throughput of flow cytometers can be significantly compromised. The penalty in sample purity and enrichment can be very severe particularly for cell sorting systems such as in fluoresce-activated cell sorting (FACS).[10]

In this paper, we demonstrate a simple fabrication and characterization method for three-dimensional (3D) flow focusing in microfluidic devices. Here, 3D focusing refers to the confinement of sample flow to a streamline at the center of the microfluidic channel. We demonstrate not only flow focusing but also focusing of the suspension in the flow over a wide range of particle size and properties. It is important to put stress on the latter because particles in the flow experience additional forces depending on their size, shape, and stiffness, thus having a tendency to settle in positions away from the center of the channel. The flow focusing force needs to counter such effects to become universally applicable to all types of biological samples. The fabrication process is compatible with the standard microfluidic device fabrication process based on soft lithography, hot embossing, or injection molding. Last but not least, the *in situ* characterization method allows us to measure, monitor, and control the extent of flow confinement without sophisticated visualization or image processing tools.

Due to the nature of laminar flow, the speed of the suspension depends on the position in the microfluidic channel. Under hydrodynamic pressure, the flow medium maintains a parabolic velocity profile, having the maximum speed at the center of the channel and zero speed at the channel wall under the no-slip boundary condition. Hydrodynamic focusing is the most popular method to confine the sample flow. It is commonly achieved by introducing a sheath flow of a higher flow rate than the sample flow. The technique has been used in commercial flow cytometers. Because of its simplicity and effectiveness, hydrodynamic focusing is also the most popular design for microfluidic devices to achieve flow confinement. Using two flanking sheath flow streams from both sides of sample flow, the sample flow and the suspension can be confined to a narrow stream in a microfluidic channel.[11] Knight *et al.* has shown that a sample flow out of a 10 μm wide channel can be confined to a width as narrow as 50 nm.[12] Various techniques of hydrodynamic focusing (*e.g.* using channel geometry and vacuum[13] or using air for sheath flow[14]) have been investigated, but most of these techniques can only confine the sample flow to a plane rather than to a cylindrical stream along the channel direction. In other words, these techniques support only 2D flow confinement, as opposed to 3D flow confinement seen in all flow cells of commercial flow cytometers.

Utilizing the properties of Dean's flow, Howell and Golden *et al.* designed "chevron-shaped" grooves on the top and bottom surfaces of flow channel to form a 3D confined flow.[15,16] Using a similar principle, Lee *et al.* designed a periodic contraction–expansion structure along the channel to induce centrifuging force to have the sheath flow wrap around the sample flow.[17] Although these designs elegantly utilize the fluid dynamic properties to achieve 3D flow confinement, the same confinement effect may not occur to the particles in the flow. Microfluidic flow cytometers in such designs have shown larger than expected coefficients of variation (CVs) because different beads and cells find their equilibrium positions away from the center. To overcome this problem, Wolff and Goranovic *et al.* achieved 3D flow confinement by designing a "chimney" structure which injected the sample flow in a perpendicular direction to the sheath flow.[18,19] Shi *et al.* introduced "sheathless" 3D hydrodynamic focusing by using standing surface acoustic waves.[20] Others

obtained 3D flow focusing using multilayered or unconventional microfluidic structures.[21–28] However, most methods reported so far require complex fabrication process and precise alignment that are incompatible with the standard processes for volume manufacturing of microfluidic devices. The major contributions of our work are (a) to demonstrate a simple and reproducible design and fabrication process to achieve 3D flow focusing in microfluidic devices that are suitable for manufacturing, (b) to achieve effective confinement for the flow itself and the particle suspensions, and (c) to develop a simple yet precise method to measure the extent of 3D particle confinement without sophisticated visualization or image processing tools. The last achievement is unique and important in flow cytometers since the extent of sample confinement depends on many parameters. Lacking *in situ* monitoring of the state of 3D confinement, the system performance can be seriously compromised.

Our design uses double-layer SU-8 lithography and PDMS molding procedure. The process produces a shorter height of sample channel aligned to the center of the main flow channel. The sample channel and the two sheath channels having a greater height than the sample channel meet at the junction before the main channel which has the same height as the sheath channel as illustrated in Fig. 1. The merge of channels of different heights produce flow confinement both in the lateral and transverse directions, resulting in 3D focused flow. Simulations and experiment show that, for different flow conditions and channel geometry, the 3D confined flow can have different cross sections, which can be characterized as an elliptical core with its long and short axes controlled by the ratio and flow rates of the sample flow and sheath flow.

Since velocity is correlated with position in a laminar flow and the position and velocity distributions of the particles in the flow matter most in all applications, we develop a method compatible with the configuration of a flow cytometer to measure the velocity of each particle directly. The distribution plot, which can be produced using the established flow cytometry software gives rise to a quantitative measurement of the actual velocity distribution of particles, which are related to the particle positions in a straightforward manner. The technique of individual particle velocity measurement is derived from the space–time coding technique developed by Wu *et al.*[29] In this paper, we adopt a similar approach to examine the velocity distribution of beads and cells to assess the effect of 3D flow focusing.

Experimental methods

Device design and fabrication

The 3D flow focusing device in our design is shown schematically in Fig. 1. The sample channel is 100 μm wide and 30 μm high; and the two sheath channels are 30 μm wide and 110 μm high. The centers for the sample channel and the sheath channels are on the same level, thus producing the geometry where the sheath channels are 40 μm above the top and below the bottom surfaces of the sample channel. The sample channel and the sheath channels meet at a junction and merge into a single (main) 100 μm wide, 110 μm high channel where fluid dynamic properties give rise to the 3D flow focusing effect as discussed in the next section. The detailed device fabrication process is described below.

The device consists of two parts, each made of polydimethylsiloxane (PDMS, Sylgard 184, Dow Corning, MI) and patterned using soft lithography process before they were bonded to form microfluidic channels. Fig. 2 (a–e) shows the process flow for both parts, defined as the top part and the bottom part for the convenience of discussion. The mold of the top part has two steps formed by double-layer SU-8 photoresist: a 40 μm high first step and a 30 μm high second step made of SU8-2050 resist and SU8-2025 resist, respectively. The mold of

the bottom part has only one layer of 40 μm SU-8 resist. Uncured PDMS was poured onto the SU-8 molds and cured at 65 °C. After curing, holes were punched through the top part to form fluid inlets and outlets, and the two PDMS parts were bonded together after UV–ozone treatment. For easy handling, the bottom part was also bonded to a glass slide. To compare the device characteristics, we also fabricated a conventional 2-dimensional flow focusing device using a similar process except that the main channel of the 2D focusing device is 100 μm high instead of 110 μm high as in the 3D focusing device. We also kept the sample channel of the same height as the main channel and the sheath channels.

Experimental setup

Syringe pumps (Harvard Apparatus, Pump Elite 11) were used to inject sample flow and sheath flow to the device at designed flow rates. Polystyrene beads of 10 μm diameter (Bangs Laboratories, Inc. Bangs Lot#: 10163) were suspended in 15% sucrose solution to neutralize the gravity effect and MCF7 cells were spiked in 1× phosphate-buffered saline (PBS) solution. Both solutions had a concentration of approximately 500 counts μL^{-1}. The same solutions as the samples without the particles were used for sheath flow.

Hydrodynamic flow focusing was first examined from the plan view and side view of the main channel using rhodamine containing methanol sample flow and methanol sheath flow. The fluorescence intensity profiles of rhodamine, measured by a CMOS camera mounted to a Nikon microscope, enabled us to visualize flow confinement for conventional 2D and the proposed 3D devices.

A flow cytometer compatible optical space–time detection system was set up to allow measurements of travel velocity of individual particles from the fluorescent signal. A 488 nm wavelength laser beam was focused to the center of the microfluidic channel over a spot spanning over positions A, B, C, as illustrated in Fig. 3. When the fluorescently-labeled particle crosses the laser illuminated spot, its fluorescence signal was focused onto an image plane where a 3-slit filter was placed in front of the detector. The positions of slits, labeled as A′, B′, C′ in Fig. 3, are conjugates of the positions A, B, C in the microfluidic channel. For a system with 50× magnification, 2.8 mm spacing between two slits corresponds to a distance of 56 μm between two adjacent points in the microfluidic channel. When a particle travels through positions A, B, C in the channel, it produces a fluorescent signal waveform showing three peaks in the photocurrent. The time interval between the adjacent peaks is equal to the division of the distance between A, B or B, C in the channel (56 μm) by the particle velocity. As a result, from the time interval between the peaks in the fluorescent signal, we can obtain the velocity of each particle in the channel. To precisely determine the timings of individual fluorescent peaks corresponding to the particle positions at A, B, C, a signal processing algorithm using digital filters was implemented in Matlab (Version 7.8.0.347, MathWorks) to remove the noise from the fluorescent signals. Since a simple relation between the velocity and the position of the bead holds in a laminar flow, knowing the particle velocity provides a direct measure of the effectiveness of flow confinement. A tight velocity distribution profile of the particles represents a tight position distribution for the particles in the channel, an indication of effective flow focusing. Also at a given flow rate, a higher average flow velocity indicates the particles are concentrated around the center of the channel where the maximum velocity occurs.

Fig. 4 shows an example of the detected signals after processing. The different peak intensities of the signal waveform were resulted from the Gaussian intensity profile of the beam spot of the excitation laser. In addition, since a key function of flow confinement is to reduce the probability of coincidental events (*i.e.* multiple particles reaching the detection region at the same time), the probability of coincidental events were characterized as a measure of the effectiveness of flow confinement.

Numerical simulation

The effects of flow focusing were investigated and modeled using COMSOL Multiphysics simulation software. The device geometry was set to be identical to the real devices, and the laminar flow model was used. In our simulation, the effect of diffusion and convection were neglected for simplicity. Particle suspensions or macromolecules are expected to leave the device in about 0.1–1 s under the flow rates of consideration. The diffusion lengths for cells and biomolecules (*e.g.* Stokes radius of 8 μm for cells and 3 nm for proteins) are estimated to be 0.08–0.25 μm for mammalian cells and 3–10 μm for proteins. Hence the effect of diffusion is negligible for biological cells but may not be negligible for molecules, something we should keep in mind when comparing the simulations with the experimental results from rhodamine samples. Since a laminar flow was established within a small distance from the junction of the sheath flow and the sample flow, the effect of convection can be neglected.

Results and discussions

Sample and sheath flow rates were set within the range of typical values for microfluidic flow cytometers (*e.g.* 1 to 4 μL min^{-1} for sample flow and 40 to 80 μL min^{-1} for sheath flow), as summarized in Table 1.

Fluidic dynamic analysis by simulation and experiment

Fig. 5 shows fluid dynamic simulation results of our device under different flow conditions. Although the sample flow and sheath flow have the same properties (*i.e.* viscosity, density, *etc.*), we represent them in different colors in simulations to help visualize the effects of 3D flow focusing. As shown in Fig. 5(b, c), an elliptically-confined sample flow is formed in our device geometry, possessing the characteristics that the lateral (*x*-direction) confinement is stronger than the transverse (*y*-direction) confinement. With increasing sheath-to-sample flow ratio, the flow focusing in the *x*-direction is enhanced while the focusing in the *y*-direction remains nearly the same. According to the simulation results, our design produces quasi-3D flow focusing, and the experiment with beads and cells in the next section indicate that significant performance improvements, in terms of uniformity of travel velocity, particle focusing, and reduction of coincidental events, can be obtained even with quasi-3D flow focusing.

Such flow focusing properties can be visualized experimentally by using fluorescent dye mixed in the sample flow. Adding rhodamine to methanol in the sample flow and using methanol for the sheath flow, we obtained micrographs showing the extent of flow confinement in the *x*- and *y*-directions. Fig. 6(a) shows the side view of a conventional 2D flow focusing design in which the uniformly distributed fluorescent intensity demonstrates the lack of flow confinement in the *y*-direction. In contrast, the fluorescent dye shows confinement in both *x*- and *y*- directions in our 3D flow focusing device, as demonstrated in Fig. 6(b–g). The results show that the widths of the confined sample flow vary under different flow conditions. Weaker confinement occurs at a lower sheath-to-sample flow ratio, consistent with the results of fluidic dynamic simulation. Fig. 6(d) and (e) show that the full-width-half-maximum (FWHM) of the sample flow in the more loosely confined *y*-direction are ~35 μm at 1 : 10 sample/sheath flow ratio and ~30 μm at 1 : 40 sample/sheath flow ratio. Fig. 6(f) and (g) show flow confinement in the *x*-direction from the top view. Similar confinement in the *x*-direction was also observed in 2D flow focusing devices although, as expected, no *y*-confinement was observed (Fig. 6(a)).

Results of beads tests

Rhodamine tests show only the flow pattern which may not truthfully represent the particle distribution since particles in the flow experience drag force, lift force and other forces that may influence their positions. These effects have been studied extensively and reported in several publications.[30–35] Therefore, using the aforementioned method to measure the velocity distribution of the particles in the fluid, we have tested the 2D and 3D flow focusing devices with beads and biological cells in the sample flow. The sample solution was made of 10 μm beads in 15% sucrose (*i.e.* 15 mg sucrose in DI water to make 100 mL solution) at a concentration of ~500 counts μL^{-1}, and introduced to both 3D and 2D flow focusing devices together with the sheath flow. Due to the well-known parabolic velocity distribution in microfluidic channels, the particle position can be evaluated from the measured velocity of beads. Using the system in Fig. 3, we obtained the velocity distribution of beads. As shown in Fig. 7, beads in the 2D flow focusing device has a coefficient of variation (CV) of 39.8%, 37.0%, and 80.7% at the sample/sheath flow rates of 1/ 40, 4/40, and 2/80 μL min^{-1}, respectively. The large CVs in the velocity distribution of beads are direct results of the lack of flow confinement in the *y*-direction. In comparison, the CVs of the velocity distribution of the 3D flow confinement device are reduced to 19.1%, 11.7%, and 10.8% under the corresponding sample/sheath flow ratios, respectively. To our best knowledge, this is the first quantitative and direct measurement for the effectiveness of a 3D flow focusing device. In addition, as shown in Table 2, the effect of flow confinement has also been demonstrated by the reduced probability of coincidental events from 9.5% in a 2D flow focused device to 3.5% in our 3D flow focused device. The result not only proves the concept of the device design but also presents a new method to characterize the velocity and spatial distribution of particles in the microfluidic channel in a manner that is compatible with microfluidic flow cytometers, without requiring a high power microscope or sophisticated visualization device.

Results of cells tests

We also characterized the devices with biological cells. Cultured and GFP-transfected MCF7 cells were spiked to a 1× PBS solution to obtain a cell concentration of ~500 counts μL^{-1}. Fig. 8 shows the measured fluorescent signal using the setup in Fig. 3 and the histograms of the velocity distribution in 2D and 3D flow focusing devices. Again, clear effects of 3D flow focusing have been demonstrated, manifested by a significant reduction in the velocity CV from 36.8% in the 2D design to 14.4% in the 3D design.

Conclusions

We have demonstrated a microfluidic 3D flow focusing device that can not only achieve 3D flow confinement but more importantly, confine particles to a tight area near the center of the channel. As a result, the suspended beads and cells show much lower CVs in velocity and position distributions as well as reduced probability of coincidental events than they do in conventional 2D confined microfluidic devices. The improved particle confinement in the microfluidic channel is highly desirable for microfluidic flow cytometers and fluorescence-activated cell sorting (FACS). The device can be fabricated using standard soft-lithography process and the design and process can be transferred to high volume fabrication processes such as hot-embossing, soft-embossing and injection molding. The design can be incorporated into many kinds of microfluidic devices that will benefit from the achievement of 3D flow confinement.

To quantitatively characterize the effect of 3D flow focusing, we have also reported a novel method to measure the velocity of each individual particle. This method is compatible with the flow cytometer setup and requires no sophisticated visualization equipment such as a

high power microscope. The technique can be used to characterize other flow focusing designs as well.

Acknowledgments

We acknowledge the technical support of the staff in the Nano3 (Nanoscience, Nanoengineering, Nanomedicine) Facility in Calit-2. One of the authors, Zhe Mei, was supported by Chinese Scholarship Council and National Natural Science Foundation of China No. 61001063. The project described was supported by Grant Number NIH 1R43RR032225. Its contents are solely the responsibility of the authors and do not necessarily represent the official views of the NIH.

References

1. Lehmann AK, Sornes S, Halstensen A. J Immunol Methods. 2000; 243:229–242. [PubMed: 10986417]
2. Pala P, Hussell T, Openshaw P. J Immunol Methods. 2000; 243:107. [PubMed: 10986410]
3. Roederer M, Brenchley JM, Betts MR, De Rosa SC. Clin Immunol. 2004; 110:199–205. [PubMed: 15047198]
4. Nunez R. CIMB, Curr Iss Mol Biol. 2001; 3:67–70.
5. Shapiro, HM. Practical flow cytometry. Wiley-Liss; 2003.
6. Jennings CD, Foon KA. Cancer Invest. 1997; 15:384–399. [PubMed: 9246163]
7. Landay A, Ohlsson-Wilhelm B, Giorgi JV. AIDS. 1990; 4:479–498. [PubMed: 2201315]
8. Dickover RE, Herman SA, Saddiq K, Wafer D, Dillon M, Bryson YJ. J Clin Microbiol. 1998; 36:1070–1073. [PubMed: 9542939]
9. Keeney M, Chin-Yee I, Nayar R, Sutherland DR. J Hematother. 1999; 8:327–329.
10. Cho SH, Godin JM, Chen CH, Qiao W, Lee H, Lo YH. Biomicrofluidics. 2010; 4:043001.
11. Reynolds O. Proc R Soc London. 1883; 35:84–99.
12. Knight JB, Vishwanath A, Brody JP, Austin RH. Phys Rev Lett. 1998; 80:3863–3866.
13. Stiles T, Fallon R, Vestad T, Oakey J, Marr D, Squier J, Jimenez R. Microfluid Nanofluid. 2005; 1:280–283.
14. Huh D, Tung YC, Wei HH, Grotberg JB, Skerlos SJ, Kurabayashi K, Takayama S. Biomed Microdevices. 2002; 4:141–149.
15. Howell PB Jr, Golden JP, Hilliard LR, Erickson JS, Mott DR, Ligler FS. Lab Chip. 2008; 8:1097–1103. [PubMed: 18584084]
16. Golden JP, Kim JS, Erickson JS, Hilliard LR, Howell PB, Anderson GP, Nasir M, Ligler FS. Lab Chip. 2009; 9:1942–1950. [PubMed: 19532970]
17. Lee MG, Choi S, Park JK. Lab Chip. 2009; 9:3155–3160. [PubMed: 19823733]
18. Klank H, Goranovic G, Kutter JP, Gjelstrup H, Michelsen J, Westergaard C. J Micromech Microeng. 2002; 12:862.
19. Wolff A, Perch-Nielsen IR, Larsen UD, Friis P, Goranovic G, Poulsen CR, Kutter JP, Telleman P. Lab Chip. 2003; 3:22–27. [PubMed: 15100801]
20. Shi J, Yazdi S, Lin SCS, Ding X, Chiang IK, Sharp K, Huang TJ. Lab Chip. 2011; 11:2319–2324. [PubMed: 21709881]
21. Sundararajan N, Pio MS, Lee LP, Berlin AA. J Microelectromech Syst. 2004; 13:559–567.
22. Simonnet C, Groisman A. Appl Phys Lett. 2005; 87:114104.
23. Chang CC, Huang ZX, Yang RJ. J Micromech Microeng. 2007; 17:1479.
24. Yang R, Feeback DL, Wang W. Sens Actuators, A. 2005; 118:259–267.
25. Mao X, Waldeisen JR, Huang TJ. Lab Chip. 2007; 7:1260–1262. [PubMed: 17896008]
26. Testa G, Bernini R. Lab Chip. 2012; 12:3670–3672. [PubMed: 22744265]
27. Kummrow A, Theisen J, Frankowski M, Tuchscheerer A, Yildirim H, Brattke K, Schmidt M, Neukammer J. Lab Chip. 2009; 9:972–981. [PubMed: 19294310]
28. Mao X, Nawaz AA, Lin SCS, Lapsley MI, Zhao Y, McCoy JP, El-Deiry WS, Huang TJ. Biomicrofluidics. 2012; 6:024113.

29. Wu TF, Mei Z, Lo YH. Lab Chip. 2012; 12:3791–3797. [PubMed: 22875178]
30. Eichhorn R, Small S. J Fluid Mech. 1964; 20:513–527.
31. Asmolov ES. J Fluid Mech. 1999; 381:63–87.
32. Di Carlo D, Irimia D, Tompkins RG, Toner M. Proc Natl Acad Sci U S A. 2007; 104:18892–18897. [PubMed: 18025477]
33. Bhagat AAS, Kuntaegowdanahalli SS, Papautsky I. Microfluid Nanofluid. 2008; 7:217–226.
34. Wu TF, Mei Z, Pion-Tonachini L, Zhao C, Qiao W, Arianpour A, Lo YH. AIP Adv. 2011:1.
35. Mei Z, Wu TF, Pion-Tonachini L, Qiao W, Zhao C, Liu Z, Lo YH. Biomicrofluidics. 2011; 5:034116.

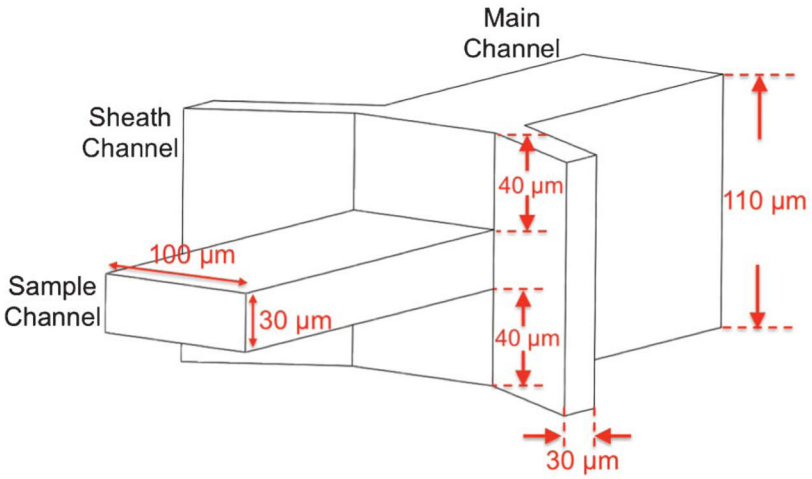

Fig. 1.
Design and dimensions of 3D flow focusing device.

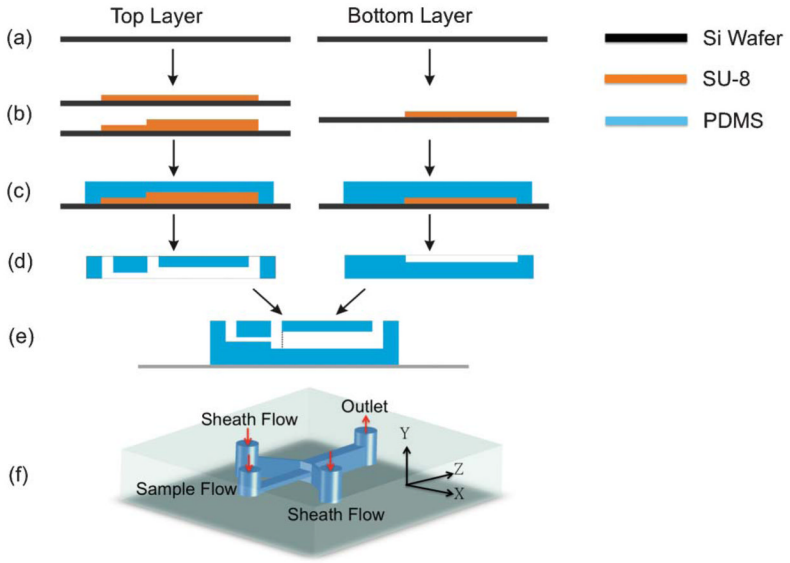

Fig. 2.

Process flow of 3D flow focusing device. (a) Si wafers as substrates for molds. (b) Forming double-step and single-step SU-8 molds. (c) Pour PDMS onto the SU-8 molds. (d) Remove PDMS from the mold. Inlet and outlet holes were punched in the top layer. (e) Two layers were bonded according to the directions in (d), with the bottom layer attached to a glass slide. (f) A view of the finished device. Coordinates are defined and will be used throughout the paper.

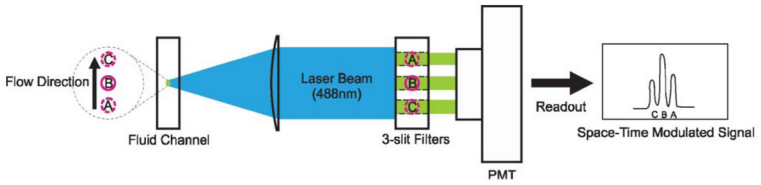

Fig. 3.

A flow cytometer compatible setup to characterize the effectiveness of flow focusing. A 488 nm laser is focused to the center of microfluidic channel by a 50 × objective lens and forms a magnified image in front of the detector. The system transforms the fluorescent signal of a particle to a plane with a 3-slit spatial filter to produce a time-domain signal with 3 distinctive peaks corresponding the particle positions A, B, C. The particle velocity can be obtained by dividing the separation between AB (or BC) with the time interval between the peaks.

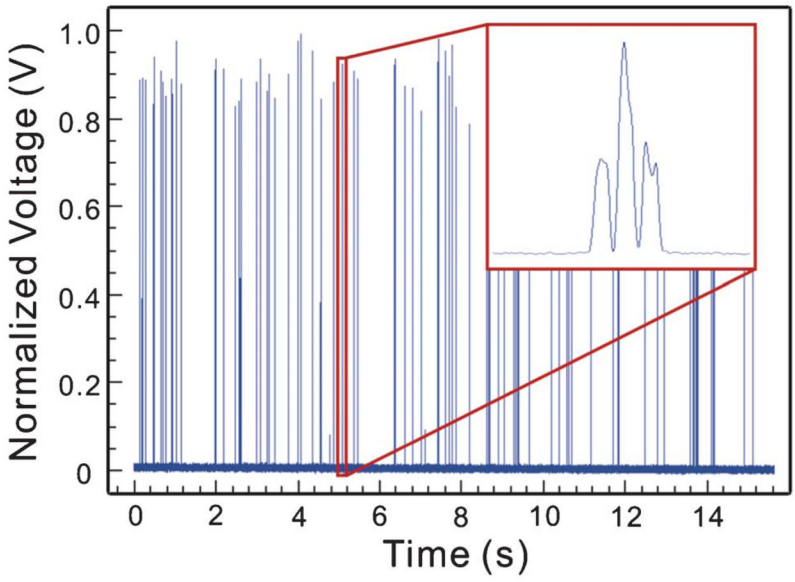

Fig. 4.

Detected fluorescent signals. The enlarged view shows the detailed waveform of the signal from a single particle traveling across positions A, B, C in Fig. 3.

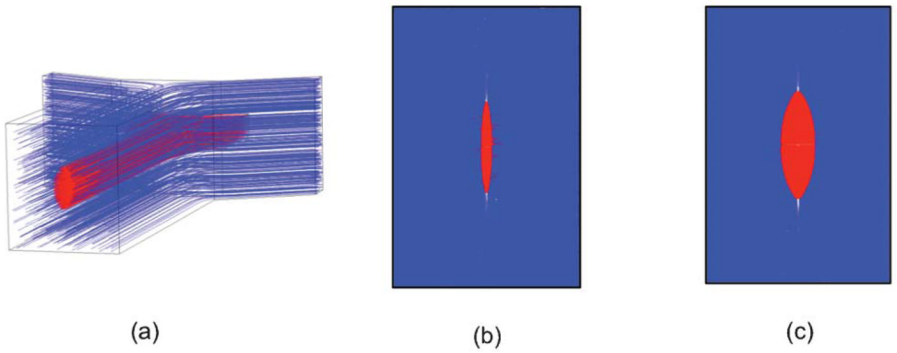

Fig. 5.

Fluidic dynamic simulations of 3D flow focusing device showing the sample flow (red) and sheath flow (blue). (a) The simulated device structure. (b, c) Cross section of the confined flow with the sample/sheath flow ratio of 1/40 μL min^{-1} and 4/40 μL min^{-1}, respectively.

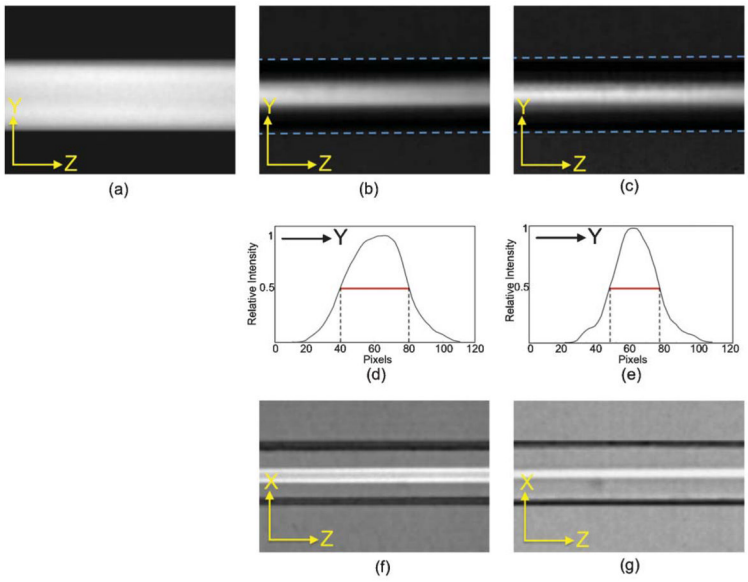

Fig. 6.

Micrographs of fluorescent intensity distributions. Side view to illustrate y-confinement for (a) 2D-design, (b) 3D-design at 1 : 10 sample/sheath flow ratio, and (c) 3D-deisgn at 1 : 40 sample/sheath flow ratio. (d), (e): Intensity profile for micrographs (b) and (c). Top view to illustrate x-confinement for (f) 3D-deisgn at 1 : 10 sample/sheath flow ratio and (g) 3D-deisgn at 1 : 40 sample/sheath flow ratio.

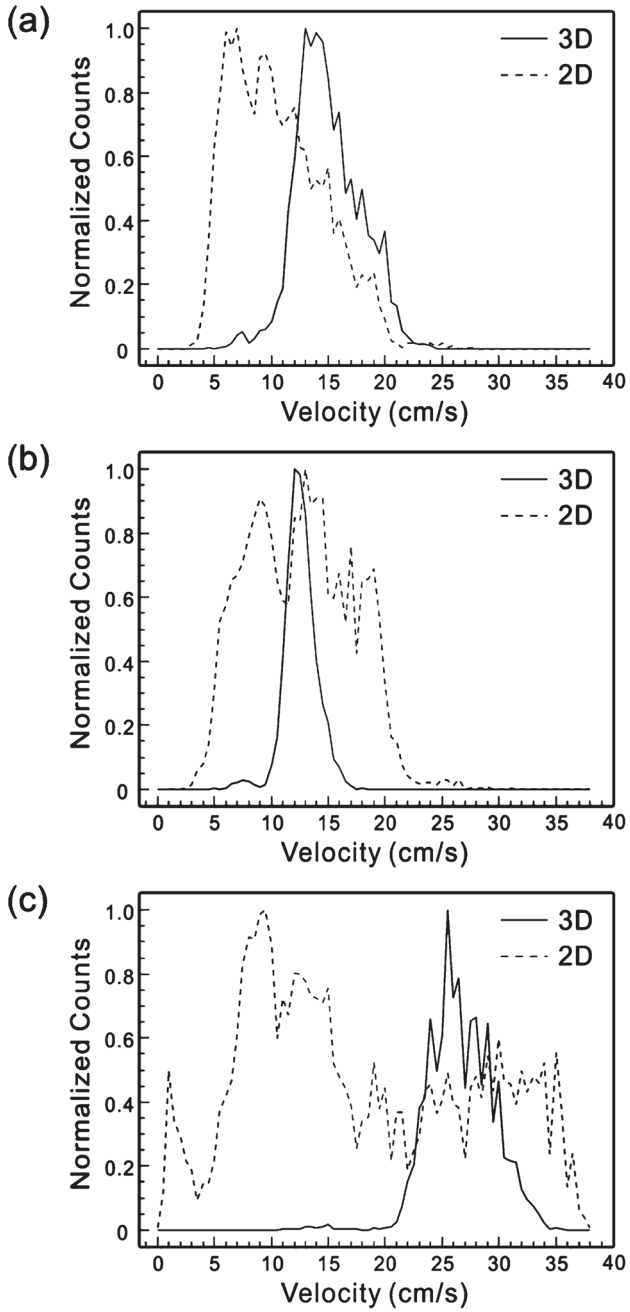

Fig. 7.

Histograms of velocity distribution of beads in 2D and 3D flow focusing devices under the sample/sheath flow rate of (a) 1/40 μL min^{-1}, (b) 4/40 μL min^{-1}, and (c) 2/80 μL min^{-1}.

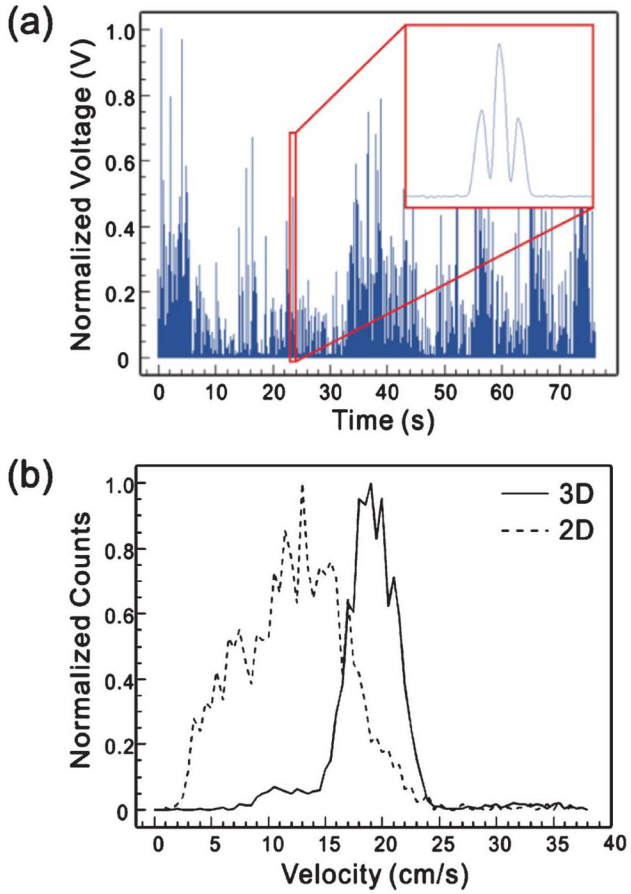

Fig. 8.

(a) Measured fluorescent signals of GFP-transfected MCF7 cells. (b) Histogram of velocity distribution of MCF7 cells under the sample/sheath flow rate of 4/40 μL min^{-1}.

Table 1

Sample and sheath flow rates used in our experiment

	Flow test	Beads test	Cell test
Sample/sheath flow rate (μL min^{-1})	1/40 and 4/40	1/40, 4/40, and 2/80	1/40 and 4/40

Table 2

CV of velocity distribution and the probability of coincidental events of beads in 2D and 3D flow focusing devices

Sample/sheath flow rate (μL min^{-1})	CV of 3D-design (%)	CV of 2D-design (%)	Coincidental event of 3D-design (%)	Coincidental event of 2D-design (%)
1/40	19.1	39.8	3.5	9.5
4/40	11.7	37.0		
2/80	10.8	80.7		